Origin of magnetism in undoped MoO_2 studied by first-principles calculations

Fenggong Wang,[1] Zhiyong Pang,[1] Liang Lin,[1] Shaojie Fang,[1] Ying Dai,[1] and Shenghao Han[1,2,*]
[1]*School of Physics, Shandong University, Jinan 250100, People's Republic of China*
[2]*School of Space Science and Applied Physics, Shandong University at Weihai, Weihai 264209, People's Republic of China*
(Received 26 January 2010; revised manuscript received 16 March 2010; published 6 April 2010)

The electronic and magnetic properties of undoped MoO_2 have been studied using first-principles calculations within both the generalized gradient approximation (GGA) and GGA+U method. The calculated results show that no magnetic moment forms in perfect MoO_2. For MoO_2 with Mo vacancies, the GGA results show some magnetic moments whereas the GGA+U (U=−1 eV for Mo) results indicate no magnetic moment forms. In the presence of type II O vacancies, both the GGA and GGA+U results show no magnetic moment can form irrespective of the vacancies concentration. Nevertheless, the type I O vacancies always lead to formation of magnetic moments which couple ferromagnetically and should be the main origin of the magnetism in undoped MoO_2. The different structural properties and the corresponding charge-density redistribution behaviors of the two inequivalent types of oxygen vacancies are the origin of the different magnetic behaviors. For the magnetic interaction, the Ruderman-Kittel-Kasuya-Yoshida interaction and the superexchange mechanism cooperatively underlie the magnetism.

DOI: 10.1103/PhysRevB.81.134407 PACS number(s): 75.50.Pp, 61.72.jd, 71.15.Mb

I. INTRODUCTION

Since the discovery of ferromagnetism in Mn-doped GaAs,[1] great effort has been made to produce intrinsic dilute magnetic semiconductors (DMSs) with Curie temperatures (T_C) at or above room temperature by doping semiconductors with transition metals (TMs).[2,3] Even though ferromagnetism has been observed in a number of systems, experimental studies have produced inconsistent results and the mechanism of the ferromagnetism in TM-doped DMSs remains unclear.[4,5] For example, the TM dopants can form clusters or secondary phases which are detrimental to intrinsic DMSs. Moreover, some experimental measurements revealed that the observed ferromagnetism in TM-doped DMSs was attributed to native vacancies.[6] Interestingly, unexpected room-temperature ferromagnetism has also been observed in undoped wideband-gap semiconducting or insulating thin films and nanoparticles such as TiO_2, HfO_2, In_2O_3, ZnO, CeO_2, SnO_2, Al_2O_3, and MgO.[7–10] This type of "d^0 magnetism"[7] has attracted much attention and provides a challenge to understand the origin of the magnetism. On one hand, the observed magnetism in TiO_2, In_2O_3, ZnO, CeO_2, SnO_2, and Al_2O_3 was attributed to anion vacancies and quantum-confinement effects.[9–11] On the other hand, it is suggested that the ferromagnetism is induced by cation vacancies in TiO_2, ZnO, MgO, HfO_2, and SnO_2, or by anion vacancies in CeO_2.[12–19] Though there is a consensus that the ferromagnetism is related with native defects, considerable controversy on the origin of the magnetism still exists.[19]

Recently, room-temperature ferromagnetism was observed in undoped MoO_2 thin films grown by pulsed laser deposition.[20] Appreciable x-ray magnetic circular dichroism structures were observed in the O 2p region, indicating a strong hybridization of O 2p-Mo 4d orbitals and a large orbital magnetic moment of O 2p states. It was also indicated that there was charge transferred from the ligand O 2p orbitals to the Mo 4d orbitals, resulting in a net magnetic polarization of O 2p orbitals. Because of the potential applications of molybdenum oxide in gas sensors, optically switchable coatings, catalysts, display devices, smart windows, and storage batteries,[21] the observed ferromagnetism in undoped MoO_2 will bring a new opportunity to the field of spintronics. However, the origin of the magnetism is still unclear and up to now no theoretical calculations have been performed to study the magnetism in undoped MoO_2. In this paper, the electronic and magnetic properties are systematically studied by first-principles density-functional theory (DFT) (Ref. 22) calculations.

II. COMPUTATIONAL METHODS

The spin-polarized DFT calculations were performed using the projector-augmented wave[22] method with a plane-wave basis set as implemented in Vienna *ab initio* simulation package (VASP) code.[23–25] The plane-wave cutoff energy was 400 eV and the exchange-correlation functional was treated by Perdew-Burke-Ernzerhof from generalized gradient approximation (GGA).[26] The valence configurations of Mo and O were $4d^5 5s^1$ and $2s^2 2p^4$, respectively. The experimental lattice parameters of molybdenum dioxide MoO_2: a =5.660 Å, b=4.860 Å, c=5.645 Å, $\alpha=\gamma=90°$, and β =120.94° were used for the calculations.[27] The MoO_2 was modeled by $2\times2\times1$ and $2\times2\times2$ supercells, which contain 48 and 96 atoms, respectively. For the Brillouin-zone sampling, $4\times5\times6$ Monkhorst-Pack[28] k mesh was used for the $2\times2\times1$ supercells while $3\times4\times3$ k mesh used for the 2 $\times2\times2$ supercells. The structure relaxations were carried out until all the atomic forces on each ion were less than 0.01 eV/Å. The calculations were also performed in GGA +U scheme.[29,30] Because Mo is not a strongly correlated system, a relative small value even a negative value of the on-site Coulomb interaction is sufficient for Mo.[31,32] Here, various values of the on-site Coulomb interaction of Mo from −1 to 1 eV are used to study the magnetic properties of MoO_2. The effective on-site exchange interaction J is set as zero and only the difference $U-J$ is meaningful.

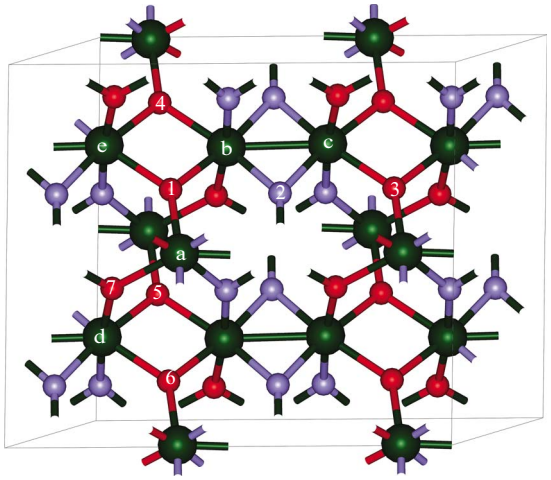

FIG. 1. (Color online) The crystalline structure of monoclinic MoO_2. The large green balls represent Mo atoms, the small red (dark gray in print) balls represent the type I O atoms, and the small blue (light gray in print) balls represent the type II O atoms, respectively.

The formation energy of the native vacancy in MoO_2 is calculated using the same method as in MgO.[19] Here, we give a detailed description again for understanding. For a neutral native vacancy, the formation energy can be defined as follows:[33]

$$E_f = (E_{tot}^v - E_{tot}^0 + n_i\mu_i)/n_i, \tag{1}$$

where E_{tot}^v and E_{tot}^0 are the total energies of the supercells with and without vacancies, n_i is the number of the atoms removed, and μ_i is the chemical potential of the corresponding atom, respectively. For example, the formation energy of an oxygen vacancy in MoO_2 is given by

$$E_f(V_O) = E_{tot}^v(V_O) - E_{tot}^0(MoO_2) + \mu_O. \tag{2}$$

In thermodynamic equilibrium, the Mo and O chemical potentials satisfy the equation,

$$\mu_{Mo} + 2\mu_O = \mu_{MoO_2}. \tag{3}$$

Here, μ_{MoO_2} is the chemical potential of MoO_2. Under extreme O-rich condition, μ_O is subject to an upper bound given by the energy of O in an O_2 molecule ($\mu_O^{max} = \frac{1}{2}\mu_{O_2}$). Correspondingly, μ_{Mo} is derived from the relation,

$$\mu_{Mo}^{min} = \mu_{MoO_2} - 2 \times \tfrac{1}{2}\mu_{O_2}. \tag{4}$$

Under extreme Mo-rich condition, μ_{Mo} is subject to an upper bound given by the energy of Mo in molybdenum metal ($\mu_{Mo}^{max} = \mu_{Mo}^0$). Correspondingly, the upper limit on the molybdenum chemical potential then results in a lower limit on the oxygen chemical potential,

$$\mu_O^{min} = \mu_{MoO_2} - \mu_{Mo}^0. \tag{5}$$

III. RESULTS AND DISCUSSIONS

In Fig. 1, the crystalline structure of perfect MoO_2 $2\times2\times1$ supercell is plotted. For convenience of discussion, the different Mo and O sites are labeled with letters and numbers. For instance, Mo^a stands for the Mo atom at site "a" while O^1 stands for the O atom at site "1" and so on. The molybdenum dioxide, which exhibits a metallic electrical conductivity, crystallizes in the distorted rutile-type monoclinic structure. In the monoclinic structure of MoO_2, there are two inequivalent types of oxygen atoms which are represented by O_I and O_{II}, respectively. Each Mo metal atom is surrounded by six oxygen atoms, forming a slightly distorted MoO_6 octahedron. The four equatorial O atoms of the distorted MoO_6 bond with the same Mo atom and the corresponding O-Mo bond length is about 2.08 Å (O_I-Mo) and 1.99 Å (O_{II}-Mo), respectively. Meanwhile, each O_I atom (O^1) bonds with three equivalent Mo atoms (Mo^a, Mo^b, and Mo^e) forming an almost planar isosceles triangle. Similarly, each O_{II} atom (O^2) bonds with three Mo atoms (Mo^b, Mo^c, and Mo^f) in a planar isosceles triangle. The top angles of the two isosceles triangle are different.

First, the electronic and magnetic properties of undoped MoO_2 are studied in the perfect MoO_2 using $2\times2\times1$ supercell. For perfect MoO_2, the calculated lattice parameters are $a=5.590$ Å, $b=4.885$ Å, and $c=5.657$ Å, which are consistent with the experimental results.[27] Generally, the Mo is in a 4+ state due to the donation of its four valence electrons to the neighboring O atoms which is in a 2− state. The total and partial density of states (DOS) of perfect MoO_2 are shown in Figs. 2(a) and 2(e), respectively. It can be clearly seen that the valence band well below the Fermi energy shows a strong hybridization of O $2p$ and Mo $4d$ orbitals whereas the conduction band at the upper part mainly arises from the Mo d orbitals. These results are consistent with previous calculations, which indicate the calculation methods are valid.[34] The perfect MoO_2 exhibits a clear metallic characteristic with Fermi energy crossing over the conduction band. Furthermore, the DOS is spin unpolarized with symmetric characteristic for the majority and minority projections of spin. The calculated total magnetic moment of the system is zero, indicating local magnetic moment cannot form in perfect MoO_2. Thus, at this point, no magnetism is induced and perfect MoO_2 is nonmagnetic.

Next, the origin of the magnetism in undoped MoO_2 is studied by generating one Mo vacancy (V_{Mo}) in the $2\times2\times1$ supercell, which leads to Mo-vacancy concentration of 6.25%. Figures 2(b) and 2(f) show the total DOS and Mo d partial DOS of MoO_2 with one Mo vacancy. Unlike that of perfect MoO_2, the total DOS shows spin-polarized metallic characteristic near the Fermi energy, which are mainly due to the spin-polarized d orbitals of Mo atom. The total magnetic moment of the system is about $0.59\mu_B$, which mainly comes from the d states of the next-neighbor Mo atoms ($0.17\mu_B$) surrounding the vacancy. Unlike MgO with Mg vacancy,[19] the magnetic moments on the neighboring O atoms are almost negligible. Basically, when a neutral Mo atom is removed, the corresponding Mo vacancy introduces four holes in the system because of the 4+ valence state of Mo. The defect states split into three degenerate t_{2g} and two degenerate e_g states under regular crystal-field effect. Considering the small magnetic moment, we infer that the four holes are nearly in the low-spin state.

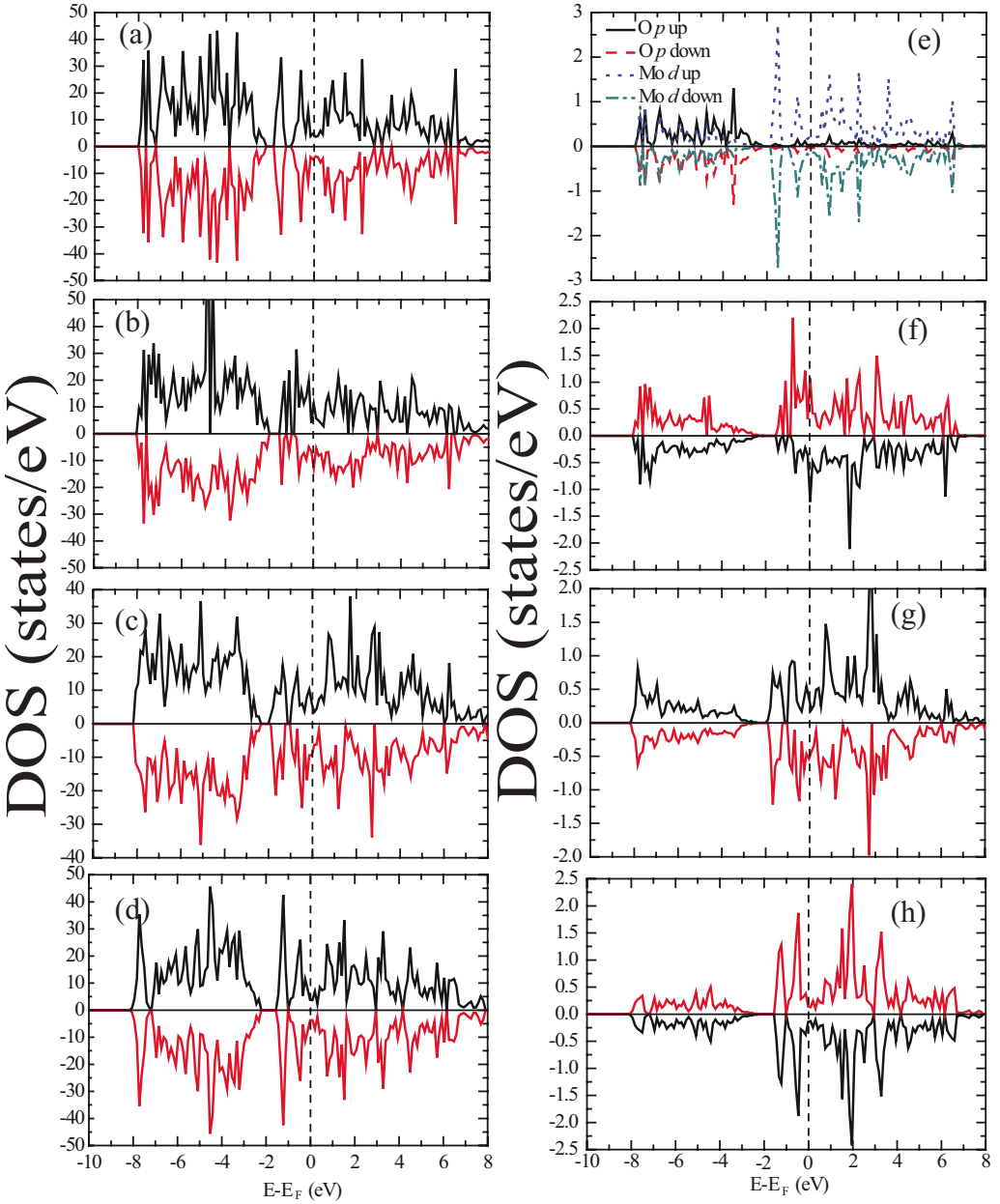

FIG. 2. (Color online) The total DOS and Mo 4*d* partial DOS of [(a) and (e)] the perfect MoO_2 crystal ($Mo_{16}O_{32}$); [(b) and (f)] MoO_2 crystal with one Mo vacancy ($Mo_{15}O_{32}$); [(c) and (g)] MoO_2 crystal with one O_I vacancy ($Mo_{16}O_{31}$); [(d) and (h)] MoO_2 crystal with one O_{II} vacancy ($Mo_{16}O_{31}$). The O 2*p* partial DOS of perfect MoO_2 is also shown in (e) for comparison. The vertical dashed line represents the Fermi energy.

To further investigate the effect of Mo-vacancy concentration, one Mo vacancy was also created in the $2\times2\times2$ supercell, corresponding to the Mo-vacancy concentration of 3.125%. As a result, the total magnetic moment is only about $0.30\mu_B$, which is smaller than that in the $2\times2\times1$ supercell. This suggests that the magnetization descends as the concentration of Mo vacancies decreases. The magnetic properties of MoO_2 with Mo vacancy are also calculated in the GGA $+U$ scheme.[29,30] Table I lists the GGA$+U$ results of the total magnetic moments of different configurations of undoped MoO_2. Four different values of the on-site Coulomb interaction from −1 to 1 eV are used to study the magnetic properties. It can be seen that the total magnetic moment induced by Mo vacancy decreases clearly when a negative U is used in the $2\times2\times1$ supercell. The magnetic moment disappears when the U is used as −1 eV. Thus, the magnetic moments induced by Mo vacancies using the GGA method is related with the overestimation of the on-site Coulomb interaction of Mo. The formation energy of Mo vacancy under O-rich conditions is 2.15 eV, which is smaller than that of Mg vacancy in MgO bulk.[19] It is indicated that there may be a concentration of Mo vacancies under extreme O-rich conditions. Nevertheless, the formation energy increases to 3.50 eV under Mo-rich conditions, leading to the concentration of Mo vacancies decreasing. Based on the above results, we infer that Mo vacancy in undoped MoO_2 may induce magnetic mo-

TABLE I. The total magnetic moments (μ_B) of different configurations of MoO_2 using GGA+U method with different U values.

	The on-site Coulomb interaction, U (eV)				
Configurations	1	0.5	0	−0.5	−1
Perfect	0.00	0.00	0.00	0.00	0.00
Mo^a vacancy	0.79	0.31	0.59	0.04	0
O^1 vacancy	0.88	0.91	0.99	1.01	1.09
O^2 vacancy	0.03	0.00	0.00	0.00	0.00

ments but should not be the main origin of the observed magnetism, especially under Mo-rich conditions.

Then the magnetism in undoped MoO_2 is also investigated in the $2\times2\times1$ supercell with oxygen vacancies (V_O). At first, one O_I atom is removed from the supercell to form an oxygen vacancy. As shown in Fig. 2(c), the total DOS shows clear spin polarization near the Fermi energy. As in MoO_2 with Mo vacancy, the spin polarization also mainly comes from the asymmetric characteristic of the majority and minority spins of Mo d orbitals [Fig. 2(g)]. The total magnetic moment of the system is $0.99\mu_B$, which is larger than that in MoO_2 with Mo vacancy. In this case, the total magnetic moment also mainly comes from the neighboring Mo atoms. Figure 3(a) shows the isosurface plot of the spin density of MoO_2 with O_I vacancy. It is evident that the spin density of O_I vacancy exhibits a planar isosceles triangle shape, showing the spin polarization strongly localized on the three-neighbor Mo atoms and the vacancy site. The remaining few magnetic moments are localized on O and Mo atoms far away. Generally, one oxygen vacancy as a donor can leave two electrons in the system. The Bader charge analysis[35] indicates that each of the three-neighbor Mo atoms has about 3.77 (3.38 in perfect MoO_2) valence electrons. This suggests that 0.39 electrons have been transferred from the O_I vacancy to each of the neighbor Mo atoms, leading to a reduced $Mo^{p+}(p<4)$ state from Mo^{4+} state. The corresponding Mo^{p+} ion has a partially occupied d subshell and the different numbers of electrons in up and down d channels of Mo^{p+} ion leads to the net magnetic moment in the system. When using GGA+U method, the total magnetic moment increases slightly with decreasing the on-site Coulomb interaction. Moreover, the total magnetic moment is about $1.09\mu_B$ even if the on-site Coulomb interaction is a negative value (−1 eV). This is different from MoO_2 with Mo vacancy, which suggests the O_I-vacancy-induced magnetic moments are stable irrespective of the on-site Coulomb interaction U. To further study the effect of O_I-vacancy concentration on the magnetism, one O_I vacancy is also created in the $2\times2\times2$ supercell. As expected, one O_I vacancy induces a magnetic moment of $0.82\mu_B$ which decreases slightly with the concentration decreasing. When three O_I vacancies are introduced in the $2\times2\times2$ supercell, the total magnetic is about $1.09\mu_B$. However, no magnetic-moment forms in MoO_2 with O_{II} vacancies irrespective of the vacancies concentration when using both GGA and GGA+U methods. Both the total DOS and Mo d partial DOS show perfect symmetric characteristics for the majority and minority projections of spin [Figs. 2(d) and 2(h)]. The different magnetic behaviors induced by the two inequivalent types of oxygen vacancies can be attributed to the different structural properties as mentioned above. Under O-rich conditions, the formation energies of O_I vacancy and O_{II} vacancy are 5.30 eV and 4.79 eV, respectively. Nevertheless, under Mo-rich conditions, the corresponding formation energies decrease much to 2.48 and 1.97 eV, implying a larger concentration of oxygen vacancies. Though the formation energy of O_I vacancy is a little larger than that of the O_{II} vacancy, there is also large concentration of O_I vacancies which can induce magnetism in undoped MoO_2. Thus, the type I O vacancy should be the main origin of the magnetism in undoped MoO_2.

As shown in Fig. 4, for the octahedral environment of molybdenum, the crystal-field splitting leads to a separation

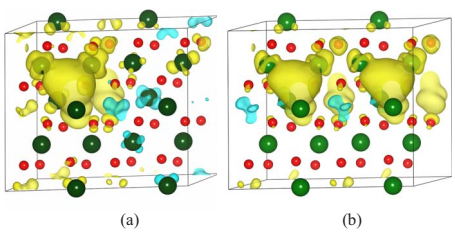

FIG. 3. (Color online) The isosurface plot of the spin density of MoO_2 with (a) one O_I vacancy and (b) two O_I vacancies at sites 1 and 3. The small red balls represent O atoms, the large green balls represent Mo atoms, and the isosurface represents the spin density, respectively.

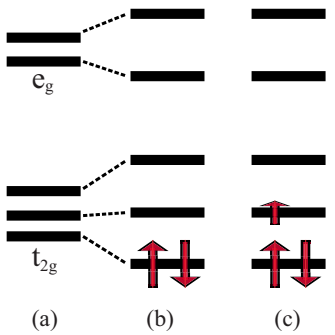

FIG. 4. (Color online) (a) The splitting of Mo 4d orbitals into t_{2g} and e_g states under regular octahedral crystal field, the occupation of the energy levels under distorted octahedral field in (b) perfect MoO_2 and (c) MoO_2 with one O_I vacancy.

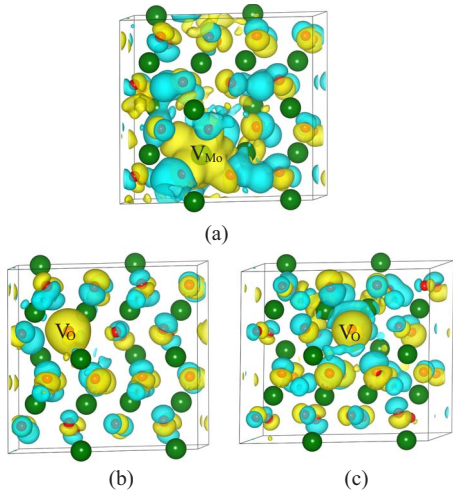

FIG. 5. (Color online) The isosurface plots of the charge redistribution of MoO_2 with (a) one Mo vacancy $[\rho(V_{Mo},MoO_2)+\rho(Mo)-\rho$ (perfect $MoO_2)]$, (b) one O_I vacancy $[\rho(V_{O_I},MoO_2)+\rho(O)-\rho$ (perfect $MoO_2)]$, and (c) one O_{II} vacancy $[\rho(V_{O_{II}},MoO_2)+\rho(O)-\rho$ (perfect $MoO_2)]$.

of the lower part of the conduction band into t_{2g} and e_g symmetry bands, and distortion of the MoO_6 octahedron leads to further splitting of the t_{2g} and e_g states, which has been proved by the experimental results.[20] For the perfect MoO_2, the Mo^{4+} ion has a partially filled $4d^2$ subshell. Correspondingly, the two electrons occupied the lowest orbital with the spin antialigning because of the Pauli principle [Fig. 4(b)]. When introducing one Mo vacancy, the corresponding four holes are strongly localized on the vacancy site, leading no magnetic moments. The isosurface plot of the charge-density redistribution of MoO_2 $2\times2\times1$ supercell with one Mo vacancy is shown in Fig. 5(a). It can be seen that the charge redistribution is mainly localized near the vacancy with electron (hole) density depleting (accumulating) at the vacancy site. The presence of Mo vacancy also leads to charge-density redistribution on the O atoms near the vacancy. Nevertheless, the net magnetic moments on the neighboring O atoms are negligible because of the delocalized characteristic of O p states. Moreover, the charge redistribution on the next-neighbor Mo atoms to the vacancy is very little, and little net magnetic-moment forms as that in perfect MoO_2. However, in the presence of one O_I vacancy, the charge redistribution leads to some electron density transferred from the vacancy to the neighbor Mo atoms although most of the introducing charge density still localizing around the O-vacancy site [Fig. 5(b)]. The transferred electron density would occupy the second lowest-energy level of Mo d orbitals, leading to the net magnetic moment in the system [Fig. 4(c)]. Furthermore, the remaining charge density is localized on the O vacancy and also lead to a large magnetic moment, as seen in Fig. 3, which is similar to the case of CeO_2 with O vacancy.[18] Surprisingly, in the case of O_{II} vacancy, electron-density transfer also takes place from the vacancy to the neighbor Mo atoms whereas no magnetic-moment forms. After full relaxation, the three-neighbor Mo atoms move nearer clearly to the vacancy site, leading to a shorter distance between the vacancy and the Mo atoms. Correspondingly, the distance between the two-neighbor Mo atoms (e.g., Mo^b and Mo^c) is about 2.39 Å, which is smaller than that in Mo metal (2.73 Å) and the two Mo atoms neighbor to O_I. According to Bader analysis,[35] the electron density transferred from the oxygen-vacancy site to the Mo atoms is more than that of the O_I-vacancy case. Unlike the case of O_I vacancy, the transferred electrons are mainly localized on the interatomic zone between the Mo atoms [Fig. 5(c)]. The different structural properties and the corresponding charge-density redistribution behaviors of the two inequivalent types of oxygen atoms are the origin of the different magnetic behaviors.

In order to investigate the magnetic interaction between oxygen-vacancy-induced magnetic moments, two oxygen vacancies are created in the $2\times2\times1$ supercell with all the atoms fully relaxed. Four different configurations (I–IV) are considered, where the two vacancies take the sites of O^1 and O^2, O^1 and O^3, O^1 and O^4, and O^1 and O^5, respectively. The distances between the vacancies are varied and the total energies of the ferromagnetic (FM) and antiferromagnetic (AFM) states are calculated. Table II shows the total-energy differences (ΔE) between the antiferromagnetic and ferromagnetic states and the total magnetic moments for all the four configurations. The positive ΔE suggests the ferromagnetic state is favored. For configuration I, the total magnetic moment is $0.61\mu_B$ and only O^1 vacancy can induce magnetic moments on the neighbor Mo atoms whereas O^2 vacancy as the type II O vacancy induces no magnetic moment. For configurations II–IV with both O vacancies belonging to the type I O vacancies, the ferromagnetic state is more favorable than the antiferromagnetic state. Moreover, the total energy of the ferromagnetic state is still lower than that of the anti-

TABLE II. The distance between the two O vacancies, total magnetic moment (M_S) of the system and largest local magnetic moment (M_L) on Mo atom, the energy difference (ΔE) between AFM and ferromagnetic (FM) states, and the corresponding magnetic coupling of different configurations of MoO_2 monoclinic cell. For configuration IV, the initial AFM state leads to FM ground state after convergence.

Configuration	d (Å)	M_S (μ_B)	M_L (μ_B)	ΔE (meV)	Magnetic coupling
I	2.76	0.61	0.15		
II	5.66	1.25	0.15	16	FM
III	2.73	1.22	0.14	8	FM
IV	3.51	1.02	0.13		FM

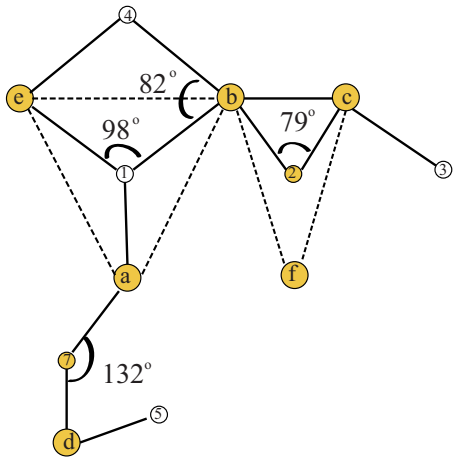

FIG. 6. (Color online) The schematic illustration of the partial structure and the magnetism mechanism of MoO_2.

ferromagnetic state even if the distance of the two O vacancies is about 5.66 Å. This indicates that a long-range ferromagnetic coupling can exist in the system to promote the collective magnetism. Nevertheless, the magnetism under thermal equilibrium conditions may not be stable at room temperature. The total magnetic moments of the configurations (II–IV) containing two O_I vacancies are $1.25\mu_B$, $1.22\mu_B$, and $1.02\mu_B$, respectively. The spin-density plot of configuration II is shown in Fig. 3(b). It is evident that two planar isosceles triangles on Mo atoms appear, which indicates that the magnetic interaction between the oxygen-vacancy-induced magnetic moments is ferromagnetic. We also studied the magnetic properties of MoO_2 in $2\times2\times1$ supercell containing three O_I vacancies at sites 1, 4, and 5, respectively. The total magnetic moment of this system is about $1.24\mu_B$ and the magnetic moments induced by the O vacancies couple ferromagnetically.

It is generally accepted that the spins of two magnetic ions are correlated due to the superexchange interaction between each of the two ions and the valence p band of the intermediate atom such as the O atom. In oxygen-deficient MoO_2, the two magnetic Mo ions form a Mo-O-Mo bond with the neighboring oxygen anion. Goodenough-Kanamori-Anderson rule[36–38] are adopted to the superexchange of MoO_2 with two O_I vacancies. The induced magnetic moments comprise two main parts, one part is localized on the reduced Mo ions and the other part is mainly localized on the vacancy site. As illustrated in Fig. 6, for configuration II with two O_I vacancies, i.e., O^1 and O^3 vacancies, the two reduced magnetic Mo ions (Mo^b and Mo^c) interact through the Mo^b-O^2-Mo^c path. The Mo^b-O^2-Mo^c bond angle is about 79°, thus the magnetic interaction between the two magnetic Mo ions is weak ferromagnetic. Similarly, in configuration III with O^1 and O^4 vacancies, the magnetic moments localized on the vacancy site interact through the V_{O^1}-Mo^b-V_{O^4} path, and the corresponding bond angle is about 82°, thus the magnetic interaction is ferromagnetic. Nevertheless, for configuration IV (O^1 and O^5 vacancies), the induced magnetic Mo ion (Mo^a and Mo^d) interact through Mo^a-O^7-Mo^d path with a bond angle of 132°. In this case, the ferromagnetic is rather weak. Surprisingly, in configuration II, the magnetic moments localized on the vacancy sites also couple ferromagnetically. As the angle is almost 180°, it cannot be explained by the indirect superexchange interaction. As MoO_2 is metallic, a high concentration of free carriers is present. Thus, similar to SnO_2 with native vacancies,[17] there is an indirect Ruderman-Kittel-Kasuya-Yoshida (RKKY) exchange coupling of magnetic moments over relatively large distance via band electrons due to the Coulomb exchange, although the oscillatory behavior is not observed. Therefore, the RKKY interaction and the superexchange cooperatively underlie the magnetism.

IV. SUMMARY

In summary, the electronic and magnetic properties of undoped MoO_2 have been studied using first-principles calculations within both the GGA and GGA+U method. The GGA results show that Mo vacancies may introduce magnetic moments in MoO_2 whereas the GGA+U results with a negative on-site Coulomb interaction (−1 eV) of Mo find no magnetic moment in MoO_2 with Mo vacancies. For MoO_2 with type II O vacancies, no magnetic moment can form irrespective of the concentration when using both GGA and GGA+U methods. Nevertheless, the type I O vacancies always lead to formation of magnetic moments which couple ferromagnetically and should be the main origin of the magnetism in undoped MoO_2. The different structural properties and the corresponding charge-density redistribution behaviors of the two inequivalent types of oxygen vacancies are the origin of the different magnetic behaviors. For the magnetic interaction, the RKKY interaction and the superexchange mechanism cooperatively underlie the magnetism.

ACKNOWLEDGMENTS

The authors are grateful for financial support from the Natural Science Foundation of China (Grants No. 10974118 and No. 10774091) and Scientific and Technological Developing Scheme of Shandong Province (Grant No. 2008GG30004004).

*Author to whom correspondence should be addressed; hansh@sdu.edu.cn

[1] H. Ohno, Science **281**, 951 (1998).
[2] T. Dietl, H. Ohno, F. Matsukura, J. Cibert, and D. Ferrand, Science **287**, 1019 (2000).
[3] T. Jungwirth, J. Sinova, J. Mašek, J. Kušera, and A. H. MacDonald, Rev. Mod. Phys. **78**, 809 (2006).
[4] H. Pan, J. B. Yi, L. Shen, R. Q. Wu, J. H. Yang, J. Y. Lin, Y. P. Feng, J. Ding, L. H. Van, and J. H. Yin, Phys. Rev. Lett. **99**, 127201 (2007).

[5] F. Wang, Z. Pang, L. Lin, S. Fang, Y. Dai, and S. Han, J. Magn. Magn. Mater. **321**, 3067 (2009).
[6] M. Gacic, G. Jakob, C. Herbort, H. Adrian, T. Tietze, S. Brück, and E. Goering, Phys. Rev. B **75**, 205206 (2007).
[7] M. Venkatesan, C. B. Fitzgerald, and J. M. D. Coey, Nature (London) **430**, 630 (2004).
[8] J. Hu, Z. Zhang, M. Zhao, H. Qin, and M. Jiang, Appl. Phys. Lett. **93**, 192503 (2008).
[9] N. H. Hong, J. Sakai, N. Poirot, and V. Brizé, Phys. Rev. B **73**, 132404 (2006).
[10] A. Sundaresan, R. Bhargavi, N. Rangarajan, U. Siddesh, and C. N. R. Rao, Phys. Rev. B **74**, 161306(R) (2006).
[11] J. M. D. Coey, M. Venkatesan, P. Stamenov, C. B. Fitzgerald, and L. S. Dorneles, Phys. Rev. B **72**, 024450 (2005).
[12] C. Das Pemmaraju and S. Sanvito, Phys. Rev. Lett. **94**, 217205 (2005).
[13] H. Peng, J. Li, S.-S. Li, and J.-B. Xia, Phys. Rev. B **79**, 092411 (2009).
[14] Q. Wang, Q. Sun, G. Chen, Y. Kawazoe, and P. Jena, Phys. Rev. B **77**, 205411 (2008).
[15] X. Zuo, S.-D. Yoon, A. Yang, W.-H. Duan, C. Vittoria, and V. G. Harris, J. Appl. Phys. **105**, 07C508 (2009).
[16] H. Peng, H. J. Xiang, S.-H. Wei, S.-S. Li, J.-B. Xia, and J. Li, Phys. Rev. Lett. **102**, 017201 (2009).
[17] G. Rahman, V. M. García-Suárez, and S. C. Hong, Phys. Rev. B **78**, 184404 (2008).
[18] X. Han, J. Lee, and H.-I. Yoo, Phys. Rev. B **79**, 100403(R) (2009).
[19] F. Wang, Z. Pang, L. Lin, S. Fang, Y. Dai, and S. Han, Phys. Rev. B **80**, 144424 (2009).
[20] P. Thakur, J. C. Cezar, N. B. Brookes, R. J. Choudhary, R. Prakash, D. M. Phase, K. H. Chae, and R. Kumar, Appl. Phys. Lett. **94**, 062501 (2009).
[21] J. Okumu, F. Koerfer, C. Salinga, and M. Wutting, J. Appl. Phys. **95**, 7632 (2004).
[22] W. Kohn and L. J. Sham, Phys. Rev. **140**, A1133 (1965).
[23] G. Kresse and D. Joubert, Phys. Rev. B **59**, 1758 (1999).
[24] G. Kresse and J. Furthmüller, Phys. Rev. B **54**, 11169 (1996).
[25] G. Kresse and J. Furthmüller, Comput. Mater. Sci. **6**, 15 (1996).
[26] J. P. Perdew, K. Burke, and M. Ernzerhof, Phys. Rev. Lett. **77**, 3865 (1996).
[27] M. Ghedira, D.-D. Chieu, and M. Marezio, J. Solid State Chem. **59**, 159 (1985).
[28] H. J. Monkhorst and J. D. Pack, Phys. Rev. B **13**, 5188 (1976).
[29] V. I. Anisimov, F. Aryasetiawant, and A. I. Lichtenstein, J. Phys.: Condens. Matter **9**, 767 (1997).
[30] S. L. Dudarev, G. A. Botton, S. Y. Savrasov, C. J. Humphreys, and A. P. Sutton, Phys. Rev. B **57**, 1505 (1998).
[31] T. Saitoh, M. Nakatake, A. Kakizaki, H. Nakajima, O. Morimoto, Sh. Xu, Y. Moritomo, N. Hamada, and Y. Aiura, Phys. Rev. B **66**, 035112 (2002).
[32] D. D. Sarma, P. Mahadevan, T. Saha-Dasgupta, S. Ray, and A. Kumar, Phys. Rev. Lett. **85**, 2549 (2000).
[33] A. Janotti and C. G. Van de Walle, Phys. Rev. B **76**, 165202 (2007).
[34] J. Moosburger-Will, J. Kündel, M. Klemm, S. Horn, P. Hofmann, U. Schwingenschlögl, and V. Eyert, Phys. Rev. B **79**, 115113 (2009).
[35] G. Henkelman, A. Arnaldsson, and H. Jonsson, Comput. Mater. Sci. **36**, 354 (2006).
[36] P. W. Anderson, Phys. Rev. **79**, 350 (1950).
[37] J. B. Goodenough, Phys. Rev. **100**, 564 (1955).
[38] J. Kanamori, J. Phys. Chem. Solids **10**, 87 (1959).